THE JOURNAL OF PHYSICAL CHEMISTRY A
A JOURNAL OF THE AMERICAN CHEMICAL SOCIETY

pubs.acs.org/JPCA
Article

A New Potential Energy Surface of the PO^+-H_2 Complex and Intermolecular Rovibrational State Calculations

Published as part of The Journal of Physical Chemistry A special issue "Computational Sciences from Africa and the African Diaspora".

Hervé Tajouo Tela, Cheikh T. Bop, François Lique, and Steve Ndengué*

Cite This: J. Phys. Chem. A 2025, 129, 6247−6260
Read Online

ABSTRACT: The recent detection of the phosphorus monoxide cation (PO^+) in the interstellar medium (ISM) has generated considerable interest in its collisional excitation and reactivity in such environments. Due to the difficulties in conducting laboratory experiments in these extreme environments, theoretical calculations have become essential to model the excitation and reactivity of PO^+. In this context, several theoretical studies have been conducted to better understand its abundance and impact on interstellar chemical processes. An important aspect of these studies is the accurate characterization of their electronic interaction with the surrounding gas constituents. We present here a new four-dimensional potential energy surface (PES) for the interaction between the PO^+ cation and the H_2 molecule, the dominant species in the cold ISM, using the explicitly correlated coupled cluster method with single, double, and perturbative triple excitations [CCSD(T)-F12**a**]. The rigid rotor PES provides a global representation of the PO^+-H_2 interaction, and presents a unique global minimum with a well depth of 1252.88 cm^{-1}. We subsequently characterized the rovibrational states of the PO^+-H_2 complex, up to a total angular momentum J of 3, by solving the nuclear Schrödinger equation with the block-induced relaxation procedure implemented in the Heidelberg Multi-Configuration Time Dependent Hartree (MCTDH) package. We obtained zero-point energies of 422.201 cm^{-1} for PO^+-*para*-H_2 and 487.805 cm^{-1} for the PO^+-*ortho*-H_2 complex. This corresponds to dissociation energies (D_0) of 830.679 and 765.075 $cm^{-1}$for PO^+-*para*-H_2 and of 487.805 cm^{-1} for the PO^+-*ortho*-H_2 complex. We hope that the present theoretical results will stimulate experimental studies of the PO^+-H_2 complex in order to validate the predictions reported in this work.

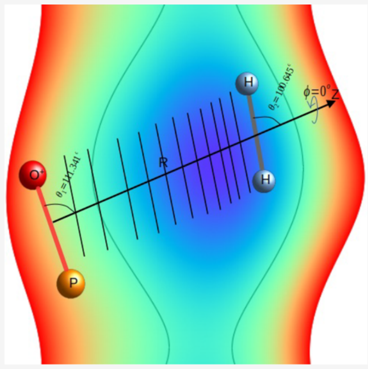

INTRODUCTION

Phosphorus (P) is a fundamental element of life, and the chemistry of phosphorus in the interstellar medium (ISM) has become increasingly important in astrobiology.[1] Species containing P element, such as PO and PH_3, have been detected in space and are believed to contribute to the formation of complex interstellar biogenic molecules.[2]

Recently, the PO^+ ion was detected by Rivilla et al.[3] in the $G + 0.693 - 0027$ molecular cloud located in the SgrB2 region of the center of the Galaxy. Its estimated abundance was found to be 4.5×10^{-12} relative to molecular hydrogen.[3] The formation of the PO^+ ion in such media occurs through the reaction of P^+ with OH or O_2.[3] The ionization of PO is also a possible path for the formation of PO^+.[3] Despite a low fractional abundance, PO^+, together with P^+, has a predominant role in the chemical network of P.

Since its detection, the rotational energy transfer of PO^+ induced by molecular hydrogen collisions[4,5] has become a focal point for studies. Indeed, H_2 is, by far, the most abundant molecule in molecular clouds and is mainly responsible for the PO^+ excitation in such media. Such studies are especially important for astronomers seeking to estimate the abundance and emission of PO^+ in the interstellar medium (ISM) using non-Local Thermodynamic Equilibrium (LTE) radiative transfer models.[6]

The study of the collisional excitation of PO^+ by H_2 requires prior determination of the interaction of PO^+ with H_2. As such, the interaction of the PO^+ ion with H_2 was modeled in recent work by Tonolo et al.[4] and Chahal et al.[5] The PO^+-H_2 potential energy surface (PES) of Tonolo et al.[4] was calculated using the explicitly correlated coupled cluster method with single, double, and perturbative triple excitations [CCSD(T)-F12**a**] method[7−9] in conjunction with the augmented correlation consistent quadruple-ζ basis set augmented by an

Received: April 18, 2025
Revised: June 18, 2025
Accepted: June 20, 2025
Published: July 2, 2025

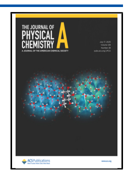

https://doi.org/10.1021/acs.jpca.5c02638
J. Phys. Chem. A 2025, 129, 6247−6260

additional d-function for P, the aug-cc-pV(Q + d)Z (hereafter AV(Q + d)Z) basis set.[10] The PO^+-H_2 PES of Chahalet al.[5] was calculated using a coupled-cluster method together with an extrapolation to the complete basis set (CBS) limit. Both PESs are considered rigid monomers.

In both situations, PES was used to study the inelastic scattering of PO^+ by H_2. Although these PESs were computed at a similar level of accuracy and looked globally similar, the scattering results turned out to be significantly different. In fact, the collisional data that resulted from the two PESs differed by more than a factor of 2 for most of the transitions.[5] Such a deviation is quite surprising and cannot be easily explained.

In light of these differences, the calculation of new collisional data based on a new PO^+-H_2 PES at the highest theoretical level possible seems essential to resolving this discrepancy. This work represents the first step in this process: computing a new PO^+-H_2 PES for the system and comparing it to the two previously developed PESs. In addition, we present calculations of the rovibrational levels of the PO^+-H_2 complex, which could serve as a reference for future experimental investigations to validate the precision of the new PES. To our knowledge, no such calculations have been reported despite the availability of recent PESs that describe the PO^+-H_2 interaction.

This work is organized as follows. In the next section, we describe the methodology and computational procedure followed for the PES calculation and quantum dynamical simulations using the MCTDH package. We then present and discuss our results, and after summarizing our work, we mention future avenues of research for this system and others.

METHODS

Potential Energy Surface. *Potential Energy Surface and Its Analytical Representation.* The interaction potential energy between $PO^+(^1\Sigma^+)$ and $H_2(^1\Sigma_g^+)$ is calculated using the rigid-rotor approximation. The H_2 bond length r_{H_2} is the internuclear distance averaged over the ground vibrational wave function (r_{H_2} = 0.767 Å). The PO^+ bond length r_{PO^+} is fixed at the distance corresponding to the equilibrium geometry of PO^+ (r_{PO^+} = 1.42499 Å),[11,12] as to the best of our knowledge, the ground vibrational wave functions are not available in the literature. The use of vibrationally averaged (r_0) instead of equilibrium geometries (r_e) is recommended in PES calculations as cross sections resulting from such interaction potentials agree better with those computed in a full-dimensional PES including vibrational effects. However, Faure et al.[13] showed that rigid-rotor PESs, based on averaged as well as equilibrium geometries, yield cross sections that agree reasonably well with experimental measurements. Furthermore, $r_0(PO^+)$ is not expected to differ strongly from $r_e(PO^+)$. Therefore, using the PO^+ equilibrium geometry instead of its vibrationally averaged internuclear distance likely has minor effects on the accuracy of the PES, and both molecules can be considered in their ground vibrational states. The PO^+-H_2 four-dimensional PES is expressed as a function of Jacobi coordinates as defined in Figure 1. Here, R denotes the distance between the centers of mass of the two monomers, the angles θ_1 and θ_2 describe the orientation of PO^+ and H_2, respectively, with the colliding axis (Z), and ϕ represents the dihedral angle between the half-planes containing PO^+ and H_2.

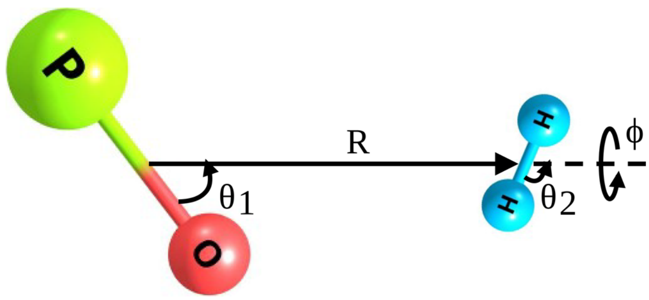

Figure 1. Definition of the PO^+-H_2 Jacobi coordinate system used to compute the PES.

For all electronic structure calculations, we use the CCSD(T)-F12a (hereafter denoted CCSD(T)-F12) in conjunction with the augmented correlation consistent triple-ζ (AVTZ) Gaussian basis set, as implemented in version 2015 of the MOLPRO quantum chemistry package.[10,14,15] For explicit correlation calculations, we used the VTZ/JKFIT and AVTZ/MP2FIT complementary basis sets of Weigen for the evaluations of the density fitting (DF) and resolution identity (RI).[16] In practice, core−valence effects were estimated, including all electrons except those in 1s of oxygen and 1s, 2s, and 2p of phosphorus. The contribution of the 2p orbital of phosphorus in the interaction energy, estimated at $R = 5.25\ a_0$, $\phi = 0°$, $\theta_2 = [80 - 120]°$, and $\theta_1 = 112°$, turns out to be less than 3 cm^{-1}. This level of theory, CCSD(T)-F12/AVTZ, is known to be very high and has been used in the literature to calculate PESs and derive bound states, differential cross sections, and integral cross sections that agree fairly well with experimental measurements.[17−20] The potential energy surface is constructed with 53 R-grid points (ranging from 4 to 20 a_0) and a 15-point Gauss-Legendre quadrature for θ_1. In addition, a 9-point Gauss-Chebyshev scheme (for ϕ) and a 5-point Gauss-Legendre scheme (for θ_2) are used in the calculations to characterize the rotational motion of H_2. The size consistency error, arising from the evaluation of the perturbative triple excitations,[8] is corrected for all geometries by subtracting from all energies the potential obtained at $R = 200\ a_0$

$$V(R, \alpha) = V(R, \alpha) - V(R = 200a_0, \alpha) \qquad (1)$$

where α stands for $\{\theta_1, \theta_2, \phi\}$. To consider the ionic nature of the collisional system, we computed additional interaction energies from $R = 20\ a_0$ to $R = 50\ a_0$ using the standard CCSD(T) method,[21] as CCSD(T)-F12 may not consistently capture the long-range interaction. The potential energies obtained with the two levels of theory exhibit differences of less than 3% at $R = 20\ a_0$. Consequently, the two data sets [$V(R \leq 20\ a_0, \alpha)$ and $V(R \geq 21\ a_0, \alpha)$] are seamlessly connected by using a cubic spline routine. For all ab initio points, the errors resulting from basis set superposition are removed using the counterpoise method.[22]

$$V(R, \alpha) = E^{H_2PO}_{PO^+-H_2}(R, \alpha) - E^{H_2PO}_{PO^+}(R, \alpha) - E^{H_2PO}_{H_2}(R, \alpha) \qquad (2)$$

Here, E_A^B stands for the energy of monomer A computed considering the atomic orbitals of all atoms in complex B. Based on different geometries, $R = 5.25\ a_0$, $\phi = 0°$, $\theta_2 = [80 - 120]°$, and $\theta_1 = 112°$, these errors were estimated to be about 15 cm^{-1}.

https://doi.org/10.1021/acs.jpca.5c02638
J. Phys. Chem. A 2025, 129, 6247−6260

To obtain an analytical representation of the PO^+-H_2 ab initio PES, we expand the interaction potential over contracted normalized bispherical harmonics as follows:

$$V(R, \theta_1, \theta_2, \phi) = \sum_{L_1L_2L} v_{L_1L_2L}(R) A_{L_1L_2L}(\theta_1, \theta_2, \phi) \quad (3)$$

eq 4 introduces the definition of bispherical harmonics,

$$A_{L_1L_2L}(\theta_1, \theta_2, \phi) = \sum_{M=0}^{\min(L_1,L_2)} \beta_i \frac{\alpha i}{(1+\delta_{M0})} \begin{pmatrix} L_1 & L_2 & L \\ M & -M & 0 \end{pmatrix} \times P_{L_1M}(\theta_1) \times P_{L_2M}(\theta_2) \cos(M\phi) \quad (4)$$

with

$$\beta_i = 2(-1)^M \left(\frac{2L+1}{2\pi}\right) \frac{1}{\sqrt{4\pi}} (-1)^{(L_1+L_2)} \quad (5)$$

and

$$\alpha_i = \frac{\sqrt{(2L_1+1)(L_2+1)}}{2} \sqrt{\frac{(L_1-M)!(L_2-M)!}{(L_1+M)!(L_2+M)!}} \quad (6)$$

Here, L_1 and L_2 are associated with the rotational motion of PO^+ and H_2, respectively. They take integer values, starting from 0, up to $L_{1\max} = 14$ and $L_{2\max} = 4$ for L_1 and L_2, respectively. By definition, $L = |L_1 - L_2|, \cdots, L_1 + L_2$ and L_2 is multiple of 2 due to the homonuclearity of H_2, with the additional constraint that $(L_1 + L_2 + L)$ is even. This resulted in a total of 122 expansion terms $v_{L_1L_2L}(R)$ to represent the PES. The relative mean deviation generated by the analytical fit (eq 3) is 1.4% at $R = 4.75\ a_0$, and it remains below 1% at all other distances. The overall RMSE of the analytical fit is 1.98 cm^{-1} for all points with R between 4 and 50 a_0 and goes up to 2.63 cm^{-1} for R between 4 and 20 a_0. The relative error is 0.14 and 0.18%. That is the analytical representation that not only describes faithfully the ab initio data in the well, but also in the long-range.

Rovibrational State Calculations with MCTDH. *MCTDH Method and the Kinetic Energy Operator.* The rovibrational spectrum of the PO^+-H_2 complex is studied with the MCTDH method.[23−26] MCTDH is a time-dependent method in which each degree of freedom (DOF) is associated with a small number of orbitals or single-particle functions (SPFs), which, through their time dependence, allow an efficient description of the quantum dynamical process. The MCTDH wave function is expanded as a weighted sum of time-dependent Hartree products:

$$\begin{aligned}\Psi(Q_1, ..., Q_f, t) &= \sum_{j_1=1}^{n_1} \cdots \sum_{j_f=1}^{n_f} A_{j_1\cdots j_f}(t) \prod_{\kappa=1}^{f} \phi_{j_\kappa}^{(\kappa)}(Q_\kappa, t) \\ &= \sum_{\Lambda} A_\Lambda \Phi_\Lambda \\ &= \sum_{j=1}^{n_k} \varphi_j^{(k)} \Psi_j^{(k)}\end{aligned} \quad (7)$$

where f is the number of DOF of the system, $Q_1, \cdots, Q_f$ are the nuclear coordinates, $A_\Lambda \equiv A_{j_1\cdots j_f}$ are the MCTDH expansion coefficients, and $\phi_{j_\kappa}^{(\kappa)}(Q_\kappa, t)$ are the n_κ SPFs associated with each degree of freedom κ (i.e., they form a time-dependent variable basis along κ).

The subsequent equations of motion for the coefficients and SPFs are derived after substituting the wave function *ansatz* into the time-dependent Schrödinger equation. To solve the equations of motion, the κ SPFs are represented on a (fixed) primitive basis, here a discrete variable representation (DVR) grid[27−29] of N_κ points:

$$\varphi_{j_\kappa}^{(\kappa)}(Q_\kappa, t) = \sum_{i_\kappa=1}^{N_\kappa} c_{i_\kappa j_\kappa}^{(\kappa)}(t) \chi_{i_\kappa}^{(\kappa)}(Q_\kappa) \quad (8)$$

where ideally the n_κ in eq 7 is such that $n_\kappa \ll N_\kappa$.

We use here, as we did in previous work on van der Waals systems,[30,31] the block-improved relaxation[32−36] method available in the Heidelberg MCTDH package, to calculate the rovibrational states of the system. This method has been described in detail before.[24,26,37] MCTDH calculations are the most efficient when the Hamiltonian is expressed as a sum of products (SOP), which is a weighted sum of the product of functions expressed in each mode (or a combination of modes). The Kinetic Energy Operator (KEO) is usually expressed in the required form when polyspherical coordinates, such as the Jacobi coordinates, are used in this study. Here, we do not work in the Body-Fixed (BF) frame but instead use the E_2 frame, as was done in previous work.[38−40] The parametrization of the Jacobi coordinates in the E_2 frame[31,40−42] is shown in Figure 2. The E_2 frame[41] is defined with its z-axis

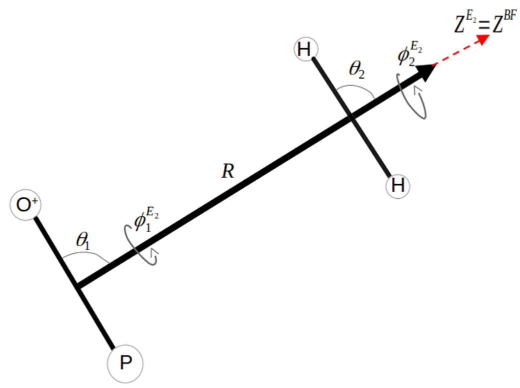

Figure 2. Jacobi E_2 spherical coordinate system for the PO^+-H_2 complex: polar and azimuthal angles $(\theta_1, \phi_1^{E_2})$ and $(\theta_2, \phi_2^{E_2})$ defining PO^+ and H_2 orientations relative to the E_2 plane.

aligned parallel to $\vec{R}$, the vector connecting the centers of mass of the two molecules. The two angles (θ_1, ϕ_1) determine the orientation of the PO^+ molecule in our E_2 frame, while the other two spherical angles (θ_2 and ϕ_2) define the orientation of the H_2 molecule.

Potential Energy Surface Representation. The PES computed in this work was originally expressed as eq 3, which is already in the appropriate sum-of-product format for MCTDH calculations. As the calculations are run in the E_2 frame, the angle ϕ is decoupled in that frame as $\phi = \phi_1 - \phi_2$. Here, ϕ_1 and ϕ_2 are the out-of-plane torsional angles, defining the rotation of the monomers around the R axis. This decoupling does not break the SOP representation but simply adds more terms to the potential representation in its MCTDH implementation.

Computational Procedure. The rovibrational state calculations were performed with the MCTDH block-improved relaxation method with a block of 4 states for each calculation,

https://doi.org/10.1021/acs.jpca.5c02638
J. Phys. Chem. A 2025, 129, 6247−6260

starting from the lowest states and progressively generating more excited states. Table 1 provides a summary of the primitive basis, its range, and the number of single-particle functions (SPFs) used in the calculations of the rovibrational states. On a 32-processor Linux cluster, the calculations ranged from 7 h for the lowest block of 4 states to about 24 h for highly excited states. These time estimates are reasonable for this type of van der Waals system, where we previously noticed that the stabilization of the time-dependent SPFs is rather slow because of the extended landscape of the wells or even their multiplicity.

Table 1. Parameters of the Primitive Basis Used for the Rovibrational Calculations of PO^+-H_2[a]

coordinate	primitive basis	number of points	range	size of SPF basis
R	FFT	96	4.0−12.0	7−10
θ_1	*KLeg*	24	0−π	10−60
ϕ_1	*K*	15	−7,7	
θ_2	*KLeg*	9	0−π	10−40
ϕ_2	*K*	11	−5,5	

[a]FFT stands for Fast Fourier Transform. *KLeg* is an extended Legendre DVR. *K* stands for the momentum representation of the azimuthal angles ϕ_1 and ϕ_2. The spherical angles θ_1 and ϕ_1 are for PO^+, and θ_2 and ϕ_2 are for H_2, both monomers in the rigid rotor approximation. The units for distances and angles are bohrs and radians, respectively.

In this work, we used the masses: 1.00784 u for H, 15.99491461956 u for O, 30.973762 u for P, and 0.00055 u for the electron and the ground state rotational constants[12,43] B_{PO^+} = 0.784343 cm^{-1} and B_{H_2} = 59.322 cm^{-1}.[44] The selection of the primitive basis set was determined through an iterative process. Various combinations of DOF numbers were tested in order to choose the most suitable primitive basis for our calculations. The ones reported in Table 1 yield a convergence of the results to better than 0.02 cm^{-1} for the low-lying states.

Additionally, the number of SPFs for each mode was increased in the calculations from a relatively small value for the lower levels to larger values for the excited states. This value grows rapidly because of the deep well of potential and the rapidly growing density of states with increasing energy. Hence, the primitive basis mentioned in Table 1 is the final configuration (largest values), and all the results presented in this study were derived from these basis parameters. FFT (Fast Fourier Transform): Applied for translational and periodic angular coordinates. *KLeg* (Legendre Polynomials in DVR form): Used for angular coordinates with defined boundaries, providing better localization. *K* (associated Legendre functions): Used in rotational coordinates with coupled angular momentum components. To ensure consistency, we performed a final variation of the single particle function (SPF) basis to achieve complete convergence in the calculations. The different ranges for the single-particle functions (SPFs) associated with ϕ_1 and ϕ_2 in Table 1 reflect the different dynamic roles of these angular coordinates in the system. Specifically, ϕ_1 is associated with the rotation of the heavier PO^+ fragment, while ϕ_2 corresponds to the rotation of the lighter H_2 molecule. As correctly noted by the referee, due to its smaller moment of inertia, H_2 rotates more rapidly and typically requires a smaller number of primitive basis functions to accurately describe its rotational motion compared to the heavier PO^+. As shown in Tables 2 and 3, convergence was achieved by increasing the size of the primitive and the SPF basis. As we discuss below, the energy E_0 represents a physical state in Table 2, while the other E_1 to E_4 correspond to nonphysical states (see below) that arise during the calculations.

Symmetry and Assignment of States. The computational procedure described above, just like in previous work[30,31] using the MCTDH algorithm in the E_2 frame, helps generate a large number of states, some physical and some unphysical. While calculations performed on slightly similar van der Waals systems (H_2O-HCN[45] or H_2O-H_2[46,47]) by other groups used a primitive basis' constraint such that K, the projection of the total angular momentum, satisfies $K = m_A + m_B$ with m_A and m_B being the projections of the angular momenta of PO^+ and H_2, respectively. The calculations with the MCTDH package do not allow for such flexibility. However, using a procedure we presented in our previous work,[30,31] we can assign and distinguish the rovibrational states from a wave function analysis. First, as we did in our H_2O-H_2's work, the Σ, Π, and ⋯ characters of the wave function can be extracted from the MCTDH calculation by looking at the output file of a single-state calculation. Then, summing the average values of the ϕ_1 and ϕ_2 DOFs (which correspond to the m_A and m_B used by

Table 2. Convergence of the Ground State Rovibrational Energy (cm^{-1}) of PO^+-*para*-H_2 for $J = 0$[a]

SPF	energy				
	E_0	E_1	E_2	E_3	E_4
10/30/20	−830.4600	*−830.4132*	*−830.3611*	*−830.2433*	*−830.2321*
10/40/20	−830.6792	*−830.6128*	*−830.6128*	*−830.4200*	*−830.4600*
10/50/20	−830.6792	*−830.6128*	*−830.6128*	*−830.4200*	*−830.4600*
10/60/20	−830.6792	*−830.6128*	*−830.6128*	*−830.4200*	*−830.4600*
7/60/20	−830.6792	*−830.6128*	*−830.6128*	*−830.4200*	*−830.4600*
10/30/30	−830.4600	*−830.4132*	*−830.3610*	*−830.2431*	*−830.2321*
10/40/30	−830.6792	*−830.6128*	*−830.6128*	*−830.4200*	*−830.4600*
10/50/30	−830.6792	*−830.6128*	*−830.6128*	*−830.4200*	*−830.4600*
7/60/30	−830.6792	*-830.6128*	*-830.6128*	*−830.4200*	*−830.4600*
10/40/40	−830.6792	*-830.6128*	*-830.6128*	*−830.4200*	*−830.4600*
10/50/40	−830.6792	*-830.6128*	*-830.6128*	*−830.4200*	*−830.4600*
7/60/40	−830.6792	*−830.6128*	*−830.6128*	*−830.4200*	*−830.4600*

[a]In the table, the first column represents the SPF basis, where $a_1/a_2/a_3$ stands for the number of SPF along the first mode R, the second combined mode *KLeg*/*K*, and the third mode *KLeg*/*K*, as suggested in Table 1. States represented in *italic* are fictitious (nonphysical) states.

Table 3. Same as Table 2 for PO^+-*ortho*-H_2

SPF	energy				
	E_0	E_1	E_2	E_3	E_4
10/30/20	−768.9351	−768.9311	−768.0751	−768.0751	−767.6843
10/40/20	−769.1010	−769.1010	−768.2520	−768.2521	−767.8155
10/50/20	−769.1010	−769.1010	−768.2520	−768.2520	−767.8152
10/60/20	−769.1010	−769.1010	−768.2520	−768.2520	−767.8152
7/60/20	−769.1010	−769.1010	−768.2520	−768.2520	−767.8152
10/30/30	−768.9351	−768.9351	−768.0751	−768.0751	−767.6843
10/40/30	−769.1010	−769.1010	−768.2520	−768.2520	−767.8152
10/50/30	−769.1010	−769.1010	−768.2520	−768.2520	−767.8152
7/60/30	−769.1010	−769.1010	−768.2520	−768.2520	−767.8152
10/40/40	−769.1010	−769.1010	−768.2520	−768.2520	−767.8152
10/50/40	−769.1010	−769.1010	−768.2520	−768.2520	−767.8152
7/60/40	−769.1010	−769.1010	−768.2520	−768.2520	−767.8152

Wang and Carrington[47]), we can determine K as $K = \langle\phi_1\rangle + \langle\phi_2\rangle$. This approach not only makes it possible to determine K but also filters out physical states from fictitious ones, which are states for which $\langle\phi_1\rangle + \langle\phi_2\rangle = K > J$.

The calculations are performed separately for the *para*-H_2 and *ortho*-H_2 nuclear spin isomers of H_2, as in spectroscopic studies (as well as in scattering studies), they can be considered as two distinct species since they are not radiatively (or collisionally) connected. In *ortho*-H_2, the spin wave function is symmetric with respect to the exchange of nuclei, while in *para*-H_2, it is antisymmetric. Since protons are Fermions, the total nuclear wave function must be antisymmetric. Consequently, the rotational wave function must be symmetric for *ortho*-H_2 and antisymmetric for *para*-H_2. This restriction imposes that the allowed rotational quantum numbers j are odd for *ortho*-H_2 and even for *para*-H_2.

In Table 2, we show the lowest 5 states of a block-improved relaxation calculation for PO^+-*para*-H_2, where only the first level of the 5 calculated is physical. In Table 3, we show the convergence tests for the PO^+-*ortho*-H_2 complex: The first physical state appears with an energy higher than the 5 presented and is therefore not displayed in Table 2.

Rovibrational State Calculations with the Coupled Channel Approach. To validate the MCTDH results, we also calculated the bound states for the total angular momenta $J = 0$ and 1 using the coupled channel approach implemented in the BOUND program.[48] To perform these calculations, we used the full spherical harmonic expansion of PO^+-H_2 PES, with 122 functions. The coupled equations were solved using the modified diabatic log-derivative method.[49] These 4D calculations were performed for both *para*- and *ortho*-H_2, and both molecules were taken as rigid rotors with rotational constants $B_0 = 59.322$ cm^{-1} for H_2 and $B_0 = 0.784343$ cm^{-1} for PO^+. A total of 26 rotational states (i.e., up to $j_1 = 25$) were included in the PO^+ basis set while the three lowest rotational states of *para*-H_2 ($j_2 = 0, 2, 4$) and *ortho*-H_2 ($j_2 = 1, 3, 5$) were considered. The calculations were performed with a propagator step size of 0.01 bohr, and the other propagation parameters were taken as the default BOUND values, where the zero-point energies were found to be 423.901 and 491.497 cm^{-1} for PO^+-*para*-H_2 and PO^+-*ortho*-H_2, respectively.

■ RESULTS AND DISCUSSION

PO^+-H_2 Interaction Potential. The global minimum of the PO^+-H_2 potential energy surface is located at an intermolecular separation of $R = 5.181$ bohr, with angular configurations defined by $\theta_1 = 111.341°$, $\theta_2 = 100.645°$, and dihedral angle $\phi = 0°$. Figure 3 displays selected 2D cuts of the PES. In Figure 3a, the plot shows the anisotropy of the interaction with the orientation of H_2 fixed at $\theta_2 = 100.645°$ and $\phi = 0°$. Figure 3b illustrates the impact of H_2 rotation on the interaction with the PO^+ geometry fixed at $\theta_1 = 111.341°$ and $\phi = 0°$. Figure 3c highlights the anisotropy of the interaction potential with the rotations of both molecules, emphasizing the anisotropy with respect to θ_1 and θ_2. Figure 3d presents the 2D contour plots of the PO^+ - H_2 PES, with the intermolecular distance fixed at $R = 5.181$ bohr and the angle $\theta_2 = 100.645°$ held constant.

These features show that 4D PES has strong anisotropies with respect to θ_1 and θ_2. Table 4 compares the equilibrium positions and well depths of the present PES with those of Tonolo et al.[4] and Chahal et al.[5] The equilibrium geometry of the PO^+-H_2 complex obtained in this work is in good agreement with previous studies. Minor differences may be due to variations in the computational methods or basis sets. In particular, the dissociation energy (D_e) found in this work (1252.88 cm^{-1}) is higher than the one reported by Chahal et al. (1230.18 cm^{-1}), while the value derived from the analytical PES of Tonolo et al. (1288 cm^{-1}) is higher than the new one. These small differences may suggest a marginally stronger interaction in some calculations, possibly due to improved correlation treatment or a more refined potential energy surface, coming from a higher density of data fitted.

The left panel of Figure 4 compares the analytical representation of the newly computed 4D PES with that of the two other PESs available in the literature near the global minimum of the PES. One can notice that the minimum reported by Tonolo et al.[4] is given with respect to the ab initio data they have computed. The value of 1234.12 cm^{-1} does not correspond to the global minimum of the PES. In Table 4, the value of 1288 cm^{-1} refers to the global minimum obtained from their analytical PES. As can be seen, the interaction potentials reported by Tonolo et al.[4] and Chahal et al.[5] show deviations from our results, underestimating and overestimating our interaction energies by up to 30 and 20 cm^{-1}, respectively. To gain insight into the discrepancies, we compare each PES with the corresponding ab initio calculations reported in each work, i.e., the CCSD(T)-F12/AV(Q + *d*)Z for Tonolo et al.,[4] the CCSD(T)/CBS* ignoring the basis set superposition errors for Chahal et al.,[5] and the CCSD(T)-F12/AVTZ. We can see that our analytical PES closely reproduces the CCSD(T)-F12/AVTZ ab initio,

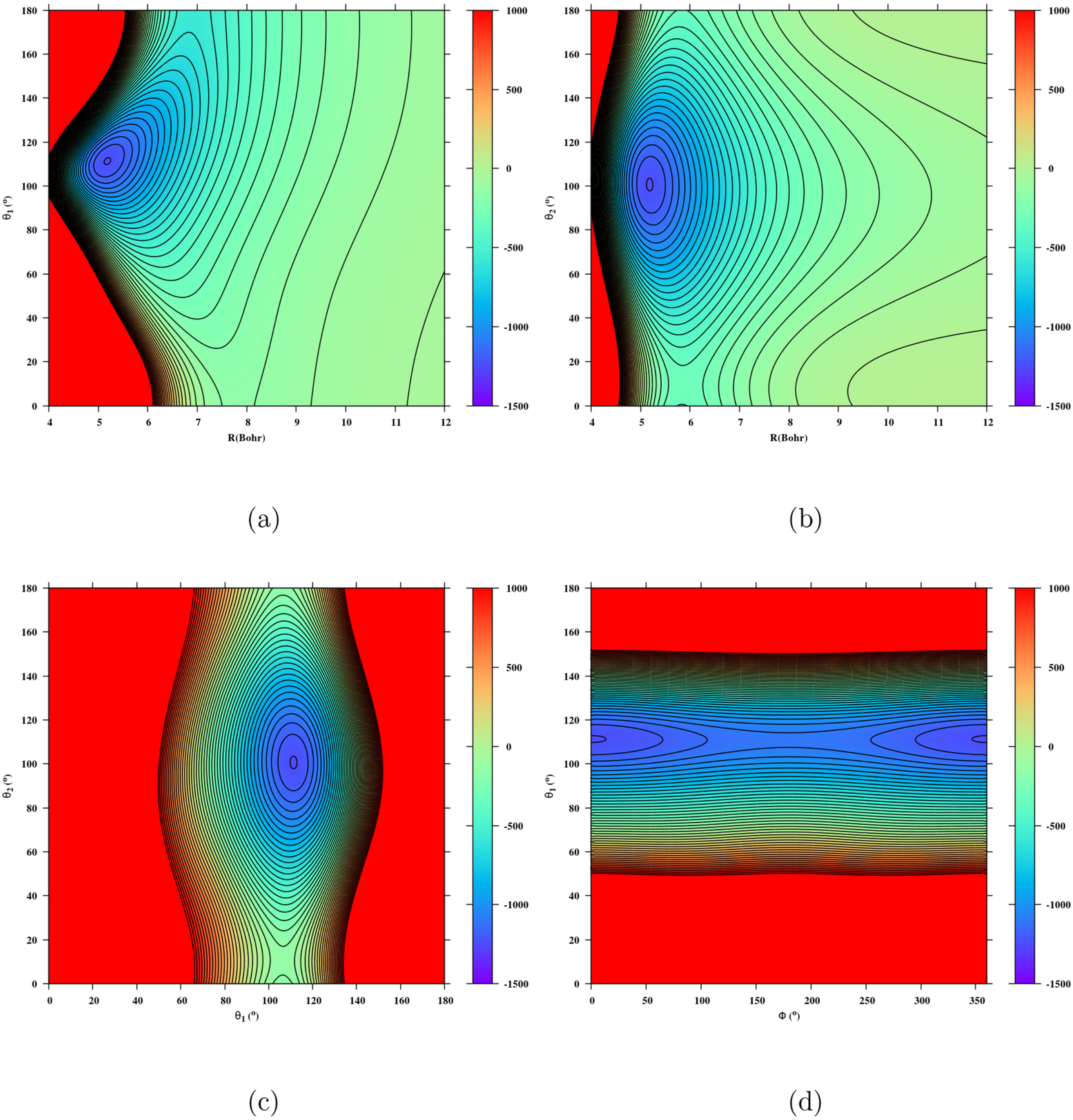

Figure 3. Contour plot of the 2D cut of the 4D PES of PO^+-H_2 for fixed θ_2 = 100.645° and ϕ = 0° (a); contour plot of the 2D cut of the 4D PES for fixed θ_1 = 111.341° and ϕ = 0° (b); contour plot of the 2D cut of the 4D PES for fixed R = 5.181 borh and ϕ = 0° (c) contour plot of the 2D cut of the 4D PES for fixed R = 5.181 bohr and θ_2 = 100.645° (d). The figures show the global minimum D_e = 1252.88 cm^{-1}.

Table 4. Equilibrium Position of the PO^+-H_2

	R (a_0)	θ_1 (°)	θ_2 (°)	ϕ (°)	D_e (cm^{-1})
this work	5.18	111.341	100.645	0	1252.88
Tonolo et al.[4]	5.29	112.291	100	0	1288
Chahal et al.[5]	5.18	110	100	0	1230.18

whereas the analytical representation of the PESs of Tonolo et al.[4] and Chahal et al.[5] fail to accurately capture the CCSD(T)-F12/AV(Q + d)Z and CCSD(T)/CBS* energy points, respectively. The deviations observed between the analytical PES of Tonolo et al.[4] and the CCSD(T)-F12/AV(Q + d)Z points are not surprising, as their PES was derived using only five H_2 orientations and none of the five H_2 orientations selected corresponded to a geometry providing the minimum energy of the PES. However, the significant discrepancies between the PES of Chahal et al.[5] and the CCSD(T)/CBS* energy points are much more surprising since Chahal et al.[5] state that their fit is of spectroscopic accuracy with deviations less than 1 cm^{-1}. The agreement between the analytical PES of Tonolo et al.,[4] Chahal et al. is not part of the agreement, and

https://doi.org/10.1021/acs.jpca.5c02638
J. Phys. Chem. A 2025, 129, 6247−6260

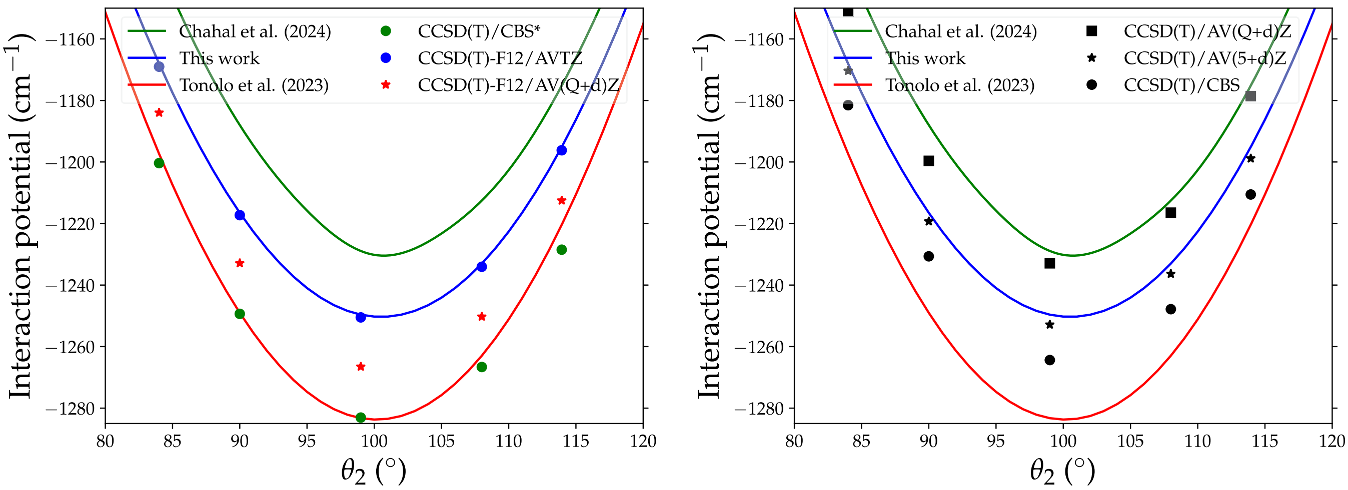

Figure 4. Comparison of the PO^+-H_2 interaction potential computed using different levels of theory and the analytical representations used in this work, in that of Tonolo et al.[4] and in the work of Chahal et al.[5] The CCSD(T)-F12/AVTZ, CCSD(T)-F12/AV(Q + *d*)Z, and CCSD(T)/CBS* levels of theory were used in this work, that of Tonolo et al.[4] and that of Chahal et al.,[5] respectively. The calculations were performed for $R = 5.25$ a_0, $\theta_1 = 112°$ and $\phi = 0°$ which is near the equilibrium position.

Table 5. Low-Energy Rovibrational Levels of PO^+-*para*-H_2 and PO^+-*ortho*-H_2 for $J = 0$[a]

PO^+-*para*-H_2					PO^+-*ortho*-H_2				
assgt.	parity	MCTDH	wgt.	BOUND	assgt.	parity	MCTDH	wgt.	BOUND
$\Sigma(0_{00})$	+	0.00	0.2646	0.00	$\Sigma(0_{00})$	+	0.00	0.2432	0.00
$\Sigma(0_{00})$	+	120.4577	0.2289	120.3893	$\Sigma(0_{00})$	−	19.1412	0.2209	18.9134
$\Sigma(0_{00})$	+	213.8560	0.230	213.7158	$\Sigma(0_{00})$	+	122.4723	0.3315	122.4533
$\Sigma(0_{00})$	−	239.9980	0.2289	239.9738	$\Sigma(0_{00})$	−	139.0331	0.3236	138.8562

[a]For PO^+-*para*-H_2, the lowest energy is -830.6792 cm^{-1}, and for PO^+-*ortho*-H_2, it is -765.0750 cm^{-1}. 'Wgt' in the table is the weight of the dominant configuration (see text for more details). The units are given in cm^{-1}.

Table 6. Same as Table 5 for $J = 1$

PO^+-*para*-H_2					PO^+-*ortho*-H_2				
assgt.	parity	MCTDH	Wgt.	BOUND	assgt.	parity	MCTDH	wgt.	BOUND
$\Sigma(1_{01})$	+	1.0982	0.2528	1.0367	$\Sigma(1_{01})$	+	1.0302	0.2717	0.9635
$\Sigma(1_{11})$	+	1.9711	0.3058	1.9059	$\Sigma(1_{11})$	+	1.8233	0.2843	1.7538
$\Sigma(1_{10})$	−	2.1730	0.3116	2.0549	$\Sigma(1_{10})$	−	1.9510	0.3082	1.8428
$\Sigma(1_{01})$	+	121.5322	0.3116	121.4197	$\Sigma(1_{11})$	−	20.2881	0.2433	20.0803
$\Sigma(1_{01})$	+	122.5592	0.2534	122.4473	$\Sigma(1_{01})$	−	21.2720	0.2433	21.0707
$\Sigma(1_{01})$	−	122.7591	0.2534	122.6133	$\Sigma(1_{10})$	+	21.5124	0.2433	21.3267
$\Sigma(1_{01})$	+	214.9682	0.2534	214.7458	$\Sigma(1_{11})$	+	123.4672	0.2433	123.4243
$\Sigma(1_{11})$	+	215.9422	0.3058	215.7697	$\Sigma(1_{11})$	+	124.3023	0.3372	124.2551
$\Sigma(1_{11})$	−	216.1514	0.2238	215.9483	$\Sigma(0_{00})$	−	124.4164	0.2927	124.3404
$\Sigma(1_{11})$	+	241.0442	0.2238	240.9168	$\Sigma(1_{01})$	−	140.1466	0.3372	139.9678
$\Sigma(1_{10})$	+	242.1163	0.2238	242.0034	$\Sigma(1_{01})$	−	141.4063	0.3082	141.2343
$\Sigma(1_{10})$	−	242.3061	0.3501	242.1085	$\Sigma(1_{10})$	+	141.6353	0.3082	141.4674

the CCSD(T)/CBS* is fortuitous, as both are approximations based on different levels of theory.

To draw a robust conclusion, the right panel of Figure 4 assesses the accuracy of the levels of theory considered in these works, namely, CCSD(T)-F12/AVTZ, CCSD(T)-F12/AV(Q + *d*)Z, and CCSD(T)/CBS* with respect to the 'gold standard' CCSD(T) method in conjunction with the CBS limit derived by extrapolating the AV(X + *d*)Z (X = T, Q, 5) basis sets. It is important to note here that we mention two separate CBS extrapolation methods. Our analytical representation and that of Chahal et al.[5] overestimate the CCSD(T)/CBS interaction potential by up to 15 and 35 cm^{-1}, respectively. The 15 cm^{-1} difference likely arises from the contribution of the *d*-functions, as the level of theory used in this work has the quality of the 'gold standard' CCSD(T) method in conjunction with a complete basis set.[8] In contrast, the analytical PES of Tonolo et al.[4] underestimates the reference calculations by up to 20 cm^{-1}. In the past, it has been shown that the use of the CCSD(T)-F12 method together with large atomic basis sets could lead to an overestimation of the interaction energy. However, in the present case, the present overestimation could certainly be mainly attributed to the limited quality of the fit that has been performed on a limited number of ab initio energy points.

If one considers the CCSD(T)/CBS interaction potential as the reference, the PES of Chahal et al.[5] appears to be the least

https://doi.org/10.1021/acs.jpca.5c02638
J. Phys. Chem. A 2025, 129, 6247−6260

Table 7. Same as Table 5 for J = 2

PO+-para-H2			PO+-ortho-H2		
assgt.	MCTDH	wgt.	assgt.	MCTDH	Wgt.
$\Sigma(2_{02})$	3.2631	0.291	$\Sigma(2_{02})$	3.0781	0.3112
$\Sigma(2_{12})$	3.9661	0.273	$\Sigma(2_{12})$	3.7600	0.2433
$\Sigma(2_{11})$	4.5722	0.331	$\Sigma(2_{11})$	4.1484	0.2825
$\Pi(2_{21})$	6.9023	0.273	$\Sigma(2_{21})$	5.5322	0.3156
$\Pi(2_{20})$	6.9023	0.324	$\Sigma(2_{20})$	6.5491	0.2342
$\Sigma(1_{10})$	7.1841	0.202	$\Sigma(1_{01})$	22.5415	0.2633
$\Sigma(1_{11})$	7.2162	0.295	$\Sigma(1_{01})$	23.3206	0.3251
$\Sigma(1_{11})$	123.6443	0.294	$\Sigma(1_{10})$	24.0392	0.2743
$\Sigma(1_{01})$	124.4981	0.302	$\Sigma(1_{10})$	26.9665	0.3314
$\Sigma(1_{01})$	125.0962	0.313	$\Sigma(1_{01})$	27.0043	0.2842
$\Sigma(1_{11})$	128.1582	0.306	$\Sigma(1_{10})$	125.4491	0.3102
$\Sigma(1_{10})$	128.1854	0.342	$\Sigma(0_{10})$	126.1883	0.3101
$\Pi(1_{10})$	133.1732	0.342	$\Sigma(1_{11})$	126.5384	0.2831

Table 8. Same as Table 5 for J = 3

PO+-para-H2			PO+-ortho-H2		
assgt.	MCTDH	wgt.	assgt.	MCTDH	wgt.
$\Sigma(3_{03})$	6.4370	0.341	$\Sigma(3_{03})$	6.1182	0.232
$\Sigma(3_{13})$	6.9381	0.294	$\Sigma(3_{13})$	6.6562	0.312
$\Sigma(3_{12})$	8.1464	0.304	$\Sigma(3_{12})$	7.4423	0.286
$\Sigma(3_{22})$	10.4795	0.290	$\Sigma(3_{22})$	9.6506	0.316
$\Sigma(3_{21})$	10.6293	0.321	$\Sigma(3_{21})$	9.7352	0.298
$\Delta(3_{31})$	13.6353	0.285	$\Sigma(3_{31})$	13.9762	0.308
$\Delta(3_{30})$	13.6351	0.307	$\Sigma(3_{30})$	13.9784	0.323
$\Sigma(3_{22})$	15.3377	0.340	$\Sigma(3_{22})$	25.8303	0.304
$\Sigma(3_{21})$	15.3402	0.328	$\Sigma(3_{21})$	26.3725	0.301
$\Sigma(1_{10})$	126.7462	0.296	$\Sigma(1_{01})$	27.8036	0.292
$\Sigma(1_{01})$	127.3897	0.303	$\Sigma(1_{10})$	30.3831	0.302
$\Sigma(1_{11})$	128.5822	0.305	$\Sigma(1_{01})$	30.5673	0.307
$\Sigma(1_{10})$	131.3671	0.285	$\Pi(1_{10})$	35.6732	0.288
$\Sigma(1_{11})$	131.4950	0.311	$\Pi(1_{01})$	35.6733	0.303
$\Sigma(1_{10})$	136.9382	0.297	$\Sigma(1_{10})$	35.8123	0.303

Table 9. Calculated Microwave Transition Frequencies (in cm^{-1}) for PO^+-*para*-H_2

transition	MCTDH	BOUND	transition	MCTDH
$1_{11} \leftarrow 0_{00}$	1.9711	1.9059	$3_{03} \leftarrow 2_{02}$	3.1739
$1_{10} \leftarrow 1_{01}$	1.0748	1.0182	$3_{13} \leftarrow 2_{12}$	2.9720
$2_{02} \leftarrow 1_{01}$	2.1648		$3_{12} \leftarrow 2_{11}$	3.5742
$2_{12} \leftarrow 1_{11}$	1.9950		$3_{12} \leftarrow 3_{03}$	1.7094
$2_{11} \leftarrow 1_{10}$	2.3992		$3_{22} \leftarrow 2_{21}$	6.5134
$2_{12} \leftarrow 1_{01}$	2.8679		$3_{21} \leftarrow 2_{20}$	7.3662
$2_{11} \leftarrow 2_{02}$	1.3091			

Table 10. Same as Table 9 for PO^+-*ortho*-H_2

transition	MCTDH	BOUND	transition	MCTDH
$1_{11} \leftarrow 0_{00}$	1.8233	1.7538	$3_{03} \leftarrow 2_{02}$	3.0401
$1_{10} \leftarrow 1_{01}$	0.9208	0.8793	$3_{13} \leftarrow 2_{12}$	2.8962
$2_{02} \leftarrow 1_{01}$	2.0478		$3_{12} \leftarrow 2_{11}$	3.2939
$2_{12} \leftarrow 1_{11}$	1.9367		$3_{12} \leftarrow 3_{03}$	1.3241
$2_{11} \leftarrow 1_{10}$	2.1974		$3_{22} \leftarrow 2_{21}$	4.1184
$2_{12} \leftarrow 1_{01}$	2.7298		$3_{21} \leftarrow 2_{20}$	3.1861
$2_{11} \leftarrow 2_{02}$	1.0703			

accurate. However, the differences in these three PESs (2−3%) as seen from the 1D cuts are relatively minor and cannot account for the large discrepancies (more than a factor of 2) observed between the collisional rate coefficients of Tonolo et al.[4] and those of Chahal et al.[5]

PO^+-H_2 Energy Levels. The rovibrational states of the complex PO^+-H_2 were obtained for the total angular momenta J = 0 to J = 3 using the methodologies described above. The calculation of the rovibrational states of a molecular system is a common way to probe the quality of the intermolecular interaction. For the PO^+-H_2 complex, there are no published experimental data to our knowledge. However, the quality of the electronic structure calculations carried out here and the experience derived from other similar van der Waals complexes suggest that the current results are a guide for future experimental investigations. In Tables 5, 6, 7, and 8, we present the lower rovibrational states of this system, reported relative to the ground rovibrational states of the PO^+-*para*-H_2 or PO^+-*ortho*-H_2 complexes, which are located at −830.6792 and −765.0750 cm^{-1}, respectively, in the MCTDH calculations, and at −828.9783 and −761.3822 cm^{-1} using the BOUND package, relative to dissociation. The close agreement between the MCTDH and BOUND results, within approximately 2 cm^{-1}, indicates that the MCTDH method provides a consistent and reliable description of the lower bound states of the system. Since BOUND is considered the reference, this close match validates the accuracy of the MCTDH calculations for these states.

The arrangement of low-energy levels reflects the anisotropy and depth of the potential energy surface, with a denser distribution near the bottom of the well. The overall structure and level positions are well reproduced, demonstrating good agreement between the two methods. Minor differences, likely due to distinct numerical treatments of the kinetic and potential energy operators, remain within acceptable limits and do not affect the overall consistency. This supports the robustness of the MCTDH approach in accurately describing bound states in weakly bound van der Waals systems.

The visualization of rovibrational states is done with an approach similar to what we did in our work on H_2O-HCN.[31] First, and as stated earlier, the K-Legendre DVR selected for the calculation helps in connecting the average value of the angular modes ϕ_1 and ϕ_2 to m_A and m_B, respectively, and then to $K = m_A + m_B$, with $= m_A$ and m_B the projection of the rotational angular momentum of each monomer on the Space-Fixed z-axis K provides the major character (Σ, Π, Δ, and ⋯) of the computed eigenstates. Next, the rotational wave function of the H_2 molecule can be described by $|j_B, m_B\rangle$ with j_B as the total angular momentum and m_B, the eigenvalue of j_B on the laboratory frame (Body-Fixed Z-axis).

The wave function can then write as follows

$$|\Psi\rangle = \sum_{j_B m_B, \chi_0} C_{j_B m_B, \chi_0} |j_B, m_B\rangle |\chi_0\rangle \tag{9}$$

where $\chi_0 = \{j_B(m_B); n_0\}$ with $j_A(m_A)$ the quantum state of PO^+ and n_0 labels the radial basis functions. The coefficients of the wave function determine the contribution of each quantum state to the overall wave function and depend on the specific rovibrational state of the system. The expansion coefficients $C_{j_B m_B \chi_0}$ from eq 9 can be expanded as follows,

$$C_{j_B m_B, \chi_0} = \sum_{-j_B}^{j_B} C_{j_B m_B, \mu} \alpha^{(j_B m_B)} \tag{10}$$

https://doi.org/10.1021/acs.jpca.5c02638
J. Phys. Chem. A 2025, 129, 6247−6260

Table 11. Calculated Rotational Constants of PO^+-*para*-H_2 (in cm^{-1}) for Each Vibrational State[a]

	MCTDH				BOUND			
state	energy	A	B	C	energy	A	B	C
ν_0	−830.6792	1.5230	0.6500	0.4480	−828.9783	1.4615	0.5925	0.4435
ν_1	−710.2215	1.6615	0.6345	0.4345	−708.5890	1.6260	0.5980	0.4320
ν_2	−616.8232	1.6345	0.6605	0.4515	−615.2624	1.6285	0.6045	0.4255
ν_3	−590.6812	1.690	0.6180	0.4280	−589.0045	1.6110	0.5240	0.4190

[a]The vibrational energies are given in units of cm^{-1}.

Table 12. Same as in Table 11 for PO^+-*ortho*-H_2

	MCTDH				BOUND			
state	energy	*A*	*B*	*C*	energy	*A*	*B*	*C*
ν_0	−765.0759	1.3721	0.5792	0.4512	−761.382	1.3161	0.5261	0.4371
ν_1	−745.9349	1.6775	0.6935	0.4535	−742.468	1.7020	0.7120	0.4550
ν_2	−642.6039	1.3895	0.5545	0.4405	−638.928	1.3590	0.5280	0.4430
ν_3	−626.0429	1.9310	0.6710	0.4420	−622.525	1.9385	0.6725	0.4395

Table 13. Characterization of the Calculated Vibrational States for PO^+-pH_2[a]

state	vibrational energy	$<R>$	ΔR	$<\theta_1>$	$\Delta\theta_1$	$<\theta_2>$	$\Delta\theta_2$
ν_0	−830.6792	5.4504	0.3748	111.8124	6.8353	100.4728	14.1348
ν_1	−710.2215	5.6321	0.4453	114.5085	12.1493	100.6235	14.3610
ν_2	−616.8232	5.7761	0.5716	113.6633	14.4697	100.3649	14.8305
ν_3	−590.6812	5.8244	0.5960	115.1591	12.2126	100.3123	14.8829

[a]The vibrational energies are given in cm^{-1}; the parameters $<R>$ and ΔR are given in bohr; $<\theta_1>$, $\Delta\theta_1$, $<\theta_2>$, and $\Delta\theta_2$ are in degrees and are defined in the text.

The coefficients $\alpha^{(j_B m_B)}$ described in eq 10 can be obtained by diagonalizing the rotational Hamiltonian of the water monomer in the $|j_B, m_B\rangle$ basis. We can then estimate the *para*-H_2 and *ortho*-H_2 rotational characters by projecting the wave function onto the rotational basis states of H_2. The weights reported in the Tables 5−8 are the highest p_i's weight for a specific state and are obtained from $p_i = \langle\Psi|\hat{P}_i|\Psi\rangle$ where $\hat{P}_i = |j_B, m_B\rangle\langle j_B, m_B|$.

The PO^+-H_2 system undergoes large-amplitude intermolecular vibrational motions. This raises questions about the average positions associated with the vibrational ground states. To quantify the deviation of the H_2 moiety from the PO^+ axis, we calculated the expected values $\langle\theta_1\rangle$ and $\langle\theta_2\rangle$, which represent the polar angles θ_1 and θ_2, respectively, for each vibrational state. These values are determined using $\langle\theta_i\rangle = \cos^{-1}\langle\cos\theta_i\rangle$, where $\langle\cos\theta_i\rangle$ is the expectation value of $\cos\theta_i$ for $i = 1, 2$. For the ground state, the results indicate $\langle\theta_1\rangle = 111.8124°$ and $\langle\theta_2\rangle = 100.4728°$ for *para*-H_2, and $\langle\theta_1\rangle = 111.7497°$ and $\langle\theta_2\rangle = 101.7328°$ for *ortho*-H_2 as reported in Tables 13 and 14. These values suggest that the molecular axis of H_2 is nearly perpendicular to the intermolecular axis of the PO^+-H_2 complex within approximately 20°. Due to the definition of the polar angles, which range from 0 to 180°, the expectation values $\langle\theta_1\rangle$ and $\langle\theta_2\rangle$ are always positive and nonzero, even when the equilibrium geometry is planar $\theta_1 = \theta_2 = 0°$. As in the case of NO^+-H_2,[50] the vibrational states are classified into distinct modes: the in-plane shear swinging mode associated with the first vibrationally excited state (ν_1), the PO^+ - H_2 symmetric stretching mode corresponding to the second vibrationally excited state (ν_2), and the PO^+ - H_2 asymmetric stretching mode linked to the third vibrationally excited state (ν_3). The corresponding modes are reported in Tables 11−14.

The rovibrational state energies obtained from our calculations are then used to extract the frequency of the PO^+-H_2 rotational transition lines. Thirteen of these transition lines are presented in Tables 9 and 10. If we rely on studies on similar systems, such as CO-H_2[51] and HCN-H_2[52] (just to mention a couple of them), the theoretical data obtained for PO^+-H_2 are also expected to be of excellent quality. In fact, the results on similar van der Waals rigid-rotor systems have generally confirmed that such high-level ab initio calculations provide an accurate representation of intermolecular interactions and can be used confidently for spectroscopic analysis.

The transition frequencies are used to obtain the rotational constants, where, following the methodology outlined by Castro et al.,[53] we have used the transition $1_{01} \leftarrow 0_{00}$, $1_{11} \leftarrow 0_{00}$ and $1_{10} \leftarrow 0_{00}$ to deduce the rotational constants *A*, *B* and *C* according to the formula: $1_{01} \leftarrow 0_{00} = B + C$, $1_{11} \leftarrow 0_{00} = A + C$ and $1_{10} \leftarrow 0_{00} = A + B$, with the added help of the near-prolate nature of the molecule which leads to an ordering of the rotational states as $A > B > C$. The rotational constants of PO^+-H_2 deduced from these calculations are presented in Tables 11 and 12. As shown by Orek et al.,[50] the rotational constants could be determined for specific vibrational states, which is what we did and show in Tables 11 and 12 for selected vibrational states.

The rotational constants exhibit notable correlations, particularly with increasing vibrational energy and the expectation value of the intermolecular distance, $<R>$. Specifically, as the vibrational energy increases, the rotational constants tend to decrease, reflecting the expansion of the molecular complex in excited vibrational states. This sensitivity underscores the strong coupling between vibrational and rotational motions. In the case of the PO^+-H_2 system, the combination of the small rotational constant of PO^+ and the presence of a deep potential well allows for the existence of a

https://doi.org/10.1021/acs.jpca.5c02638
J. Phys. Chem. A 2025, 129, 6247−6260

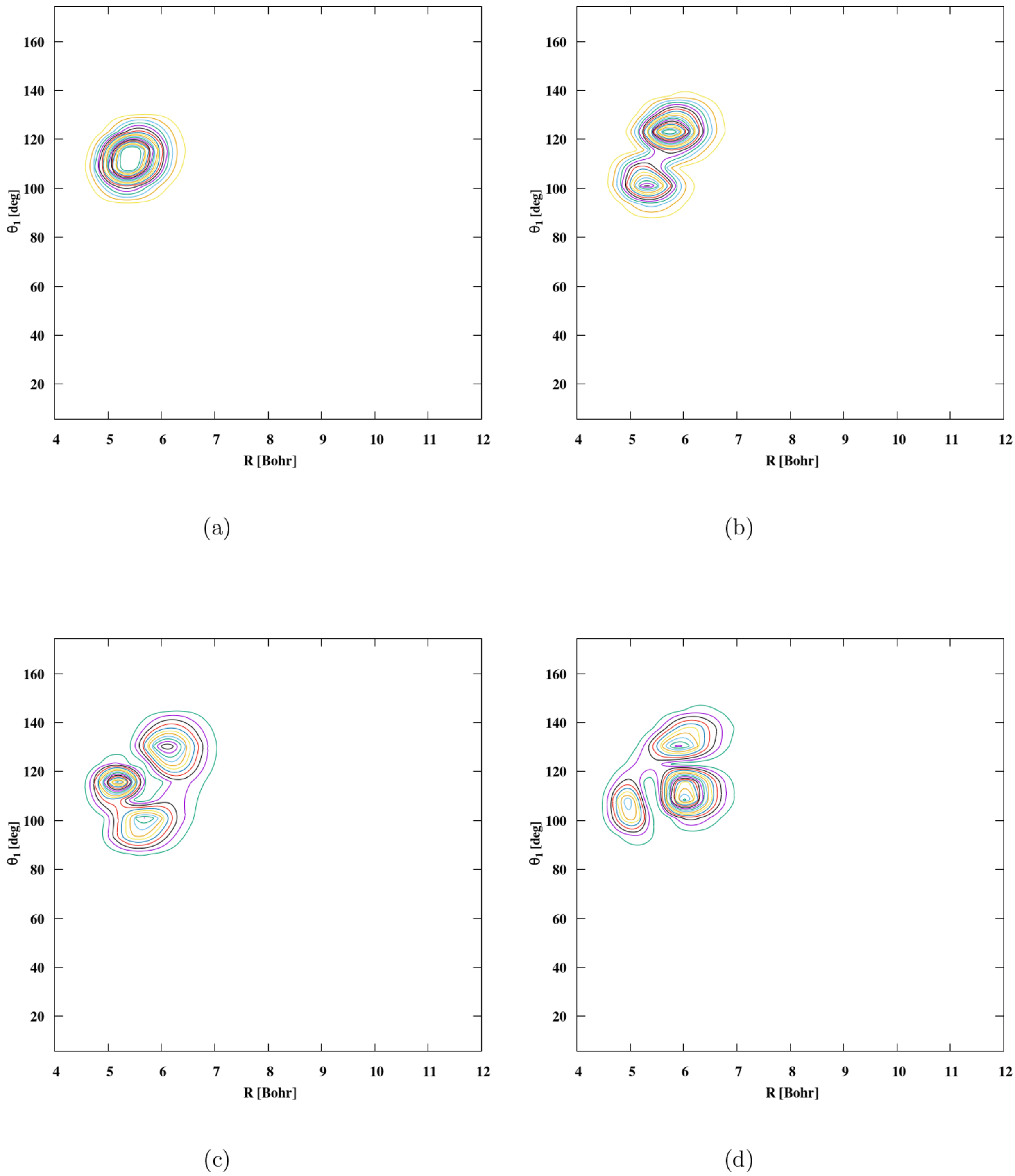

Figure 5. 2D cuts of the wave function's density of the lowest 4 states of PO^+-*para*-H_2. (a) $E = 0$ cm^{-1}. (b) $E = 120.4577$ cm^{-1}. (c) $E = 213.8560$ cm^{-1}. (d) $E = 239.9980$ cm^{-1}.

large number of vibrational states for $J = 0$. A similar trend has been observed in other complexes of ion molecules, such as NO^+-H_2,[50] further confirming the generality of this behavior in weakly bound molecular dimers containing a molecular ion.

The determination of the intermolecular vibrational states proved to be a particularly challenging task. As shown in Tables 13 and 14, these states were identified through a detailed analysis of contour plots that represent the wave functions of the corresponding eigenstates in carefully chosen internal coordinates. Additionally, wavepacket propagation provides an alternative approach for characterizing rovibrational states. In this work, this method[47] was used by evaluating the average contributions of each degree of freedom.

Our methodology for characterizing vibrational states remained consistent with previously established approaches, particularly those successfully applied in the identification of vibrational states for H_2O−HCN[31] and H_2O−H_2.[47]

The characterization of intermolecular vibrational states is crucial to understanding the quantum dynamics of weakly bound molecular complexes. However, excitation energies alone are often insufficient; they must be assigned to fundamental vibrations. This requires access to wave functions,

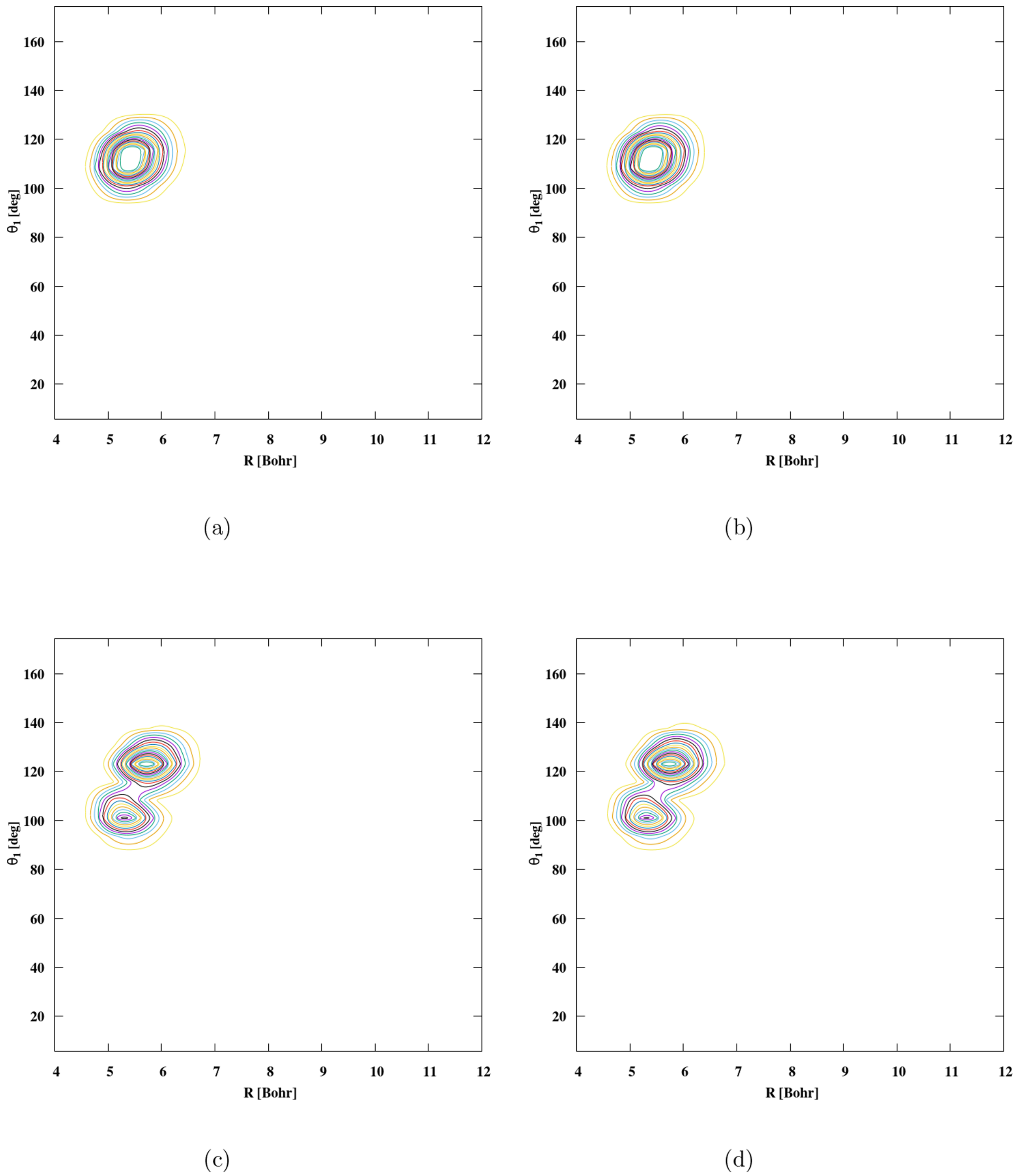

Figure 6. 2D cuts of the density (R, θ_1) of the wave functions of PO^+-*ortho*-H_2: (a) $E = 0$ cm^{-1}, (b) $E = 19.1412$ cm^{-1}, (c) $E = 122.4723$ cm^{-1}, and (d) $E = 139.0331$ cm^{-1}.

Table 14. Same as Table 13 for PO^+-oH_2

state	vibrational energy	$<R>$	ΔR	$<\theta_1>$	$\Delta\theta_1$	$<\theta_2>$	$\Delta\theta_2$
ν_0	−765.0759	5.4524	0.3716	111.7497	6.7723	101.7328	12.5415
ν_1	−745.934	5.4705	0.3742	111.8342	6.8583	101.7340	12.7338
ν_2	−642.6039	5.6095	0.4390	114.3594	11.9117	101.5396	13.5519
ν_3	−626.0429	5.6302	0.4446	114.5564	12.0836	101.4435	12.860

which are obtained through relaxation procedures. During relaxation, the initial wave packet evolves and converges toward the stationary bound states, with each resulting eigenstate saved as a separate file in the output representing the corresponding wave function. The analysis of wave

https://doi.org/10.1021/acs.jpca.5c02638
J. Phys. Chem. A 2025, 129, 6247−6260

functions provides insight into the nature of bound states and the interplay between rotational and vibrational motions.

To explore these aspects, we present the wave functions for each system configuration in Figures 5 and 6. Additional insights are obtained by examining two-dimensional contour plots of the wave function in carefully selected coordinate pairs. For each state, we analyze 2D contour plots as functions of (R, θ_1), with specific visualizations for PO^+-*para*-H_2 and PO^+-*ortho*-H_2 provided in Figures 5a and 6a. In Tables 13 and 14 the quantities ΔR and $\Delta\theta_i$ reported correspond to the root-mean-square (rms) amplitudes of the coordinate fluctuations. These values are used to describe the spatial extent of vibrational motion and the variation of the coordinates from one state to another. In the ground state, the wave function is localized at the global minimum, with H_2 moving around PO^+ in a manner consistent with localization at $<R\geq$ 5.450 bohr and $<\theta_1\geq$ 111.812°. Figures 5b,c and 6b,c show the contour plots of the wave function of the first excited states for PO^+-*para*-H_2 and PO^+-*ortho*-H_2. In particular, there is a distinct change in the nature of the complex between the ground and first vibrational states for $J = 0$, indicating a sudden change in the geometry between these states. Figure 5c,d show the wave functions of the second and third excited states of *para*-H_2 with two nodes with respect to the intermolecular distance R and θ_1. In Figure 6, the same characterization has been done, as shown in Figure 6a−d, for *ortho*-H_2, simplifying the process of recognizing the intermolecular stretch and its various excitations as reported in Table 14. In the *ortho*-H_2 configuration, the ground state and the first excited state appear to be visually identical, showing a stable wave function without a node. Likewise, the second and third excited states exhibit a single node following R and θ_1. However, the task of characterization of states primarily associated with excitations of the angular degrees of freedom in the complex proves to be considerably more demanding. Unfortunately, there is a lack of spectroscopic data in the existing literature on excited intermolecular vibrational states of the PO^+-H_2 complex, precluding any comparison with theoretical results.

CONCLUSIONS

We presented a new intermolecular PES for the PO^+-H_2 van der Waals system, calculated at the CCSD(T)-F12 level of theory. Using the MCTDH method, we computed and analyzed the low-lying rovibrational levels of this system for values of the total angular momentum quantum number J between 0 and 3. Using an approach presented before,[30,31] it is straightforward to assign the rovibrational states of the PO^+-H_2 complex based on the value of K, the projection of the total angular momentum J. To the best of our knowledge, this is the first time that the MCTDH approach has been used for rovibrational calculations on this type of van der Waals complex.

Because of the small rotational constant of PO^+, a large rotational basis is required to converge the rovibrational states. When we add this to the dimensionality of the problem, the calculations for this type of system are challenging to converge with standard computation methods, such as the one implemented in BOUND, and would therefore benefit from the better scalability of algorithms such as MCTDH. As such, one of the objectives of this work was to offer the MCTDH method described here as a possible alternative for the systematic study of similar systems. Our results could also be expected to guide future experimental work on this complex.

Finally, as mentioned in the Introduction, the main purpose of this work was to build a new PES that could later be used to settle the debate that arises from the large differences observed in cross sections and collision rate coefficients obtained by Tonolo et al.[4] and Chahal et al.[5] To validate the accuracy of the PES, we performed parallel calculations using both the MCTDH and BOUND packages. The zero-point energies obtained with MCTDH were 422.201 cm^{-1} for PO^+- *para*-H_2 and 487.805 cm^{-1} for PO^+-*ortho*-H_2, while the BOUND package produced 423.901 and 491.497 cm^{-1}, respectively. The close agreement between the two methods shows that both MCTDH and bound calculations converge. For future work, we will employ both approaches, with particular emphasis on MCTDH, which is well-suited for treating systems with a high density of states and delivering benchmark-quality results.

AUTHOR INFORMATION

Corresponding Author

Steve Ndengué − *Department of Physics and Astronomy, Haverford College, Haverford, Pennsylvania 19041, United States;* orcid.org/0000-0001-7136-3827;
Email: sndengue@haverford.edu

Authors

Hervé Tajouo Tela − *ICTP-East African Institute for Fundamental Research, University of Rwanda, P.O. Box 3900 Kigali, Rwanda*

Cheikh T. Bop − *Physics Department, Khalifa University, P.O. Box 127788 Abu-Dhabi, United Arab Emirates; Univ. Rennes, CNRS, IPR (Institut de Physique de Rennes) − UMR 6251, F-35000 Rennes, France;* orcid.org/0000-0003-2369-1601

François Lique − *Univ. Rennes, CNRS, IPR (Institut de Physique de Rennes) − UMR 6251, F-35000 Rennes, France;* orcid.org/0000-0002-0664-2536

Complete contact information is available at:
https://pubs.acs.org/10.1021/acs.jpca.5c02638

Author Contributions

Hervé Tajouo Tela performed the rovibrational calculations, analyzed the results, and contributed to the redaction of the manuscript. Cheikh T. Bop and François Lique computed the Potential Energy Surface and contributed to the analysis of the results and the redaction of the manuscript. Steve Ndengué contributed to the conceptualization and design of the work, the analysis of the results, and the redaction of the manuscript.

Notes

The authors declare no competing financial interest.

ACKNOWLEDGMENTS

The authors would like to acknowledge the support from CINECA for the computational time allocated to ICTP-EAIFR. H.T.T. acknowledges the financial support from the Office of External Activities of the Abdus Salam International Centre for Theoretical Physics: (Ph.D. fellowship No. AF-16/20-04)/ICTP-OEA.

REFERENCES

(1) Fernández-Ruz, M.; Jiménez-Serra, I.; Aguirre, J. A theoretical approach to the complex chemical evolution of phosphorus in the interstellar medium. *Astrophysical Journal* **2023**, *956*, 47.

(2) Fontani, F. Observations of phosphorus-bearing molecules in the interstellar medium. *Front. Astron. Space Sci.* **2024**, *11*, No. 1451127.
(3) Rivilla, V. M.; García De La Concepción, J.; Jiménez-Serra, I.; Martín-Pintado, J.; Colzi, L.; Tercero, B.; Megías, A.; López-Gallifa, A.; Martínez-Henares, A.; Massalkhi, S.; et al. Ionize Hard: Interstellar PO^+ Detection. *Frontiers in Astronomy and Space Sciences* **2022**, *9*, No. 829288.
(4) Tonolo, F.; Bizzocchi, L.; Rivilla, V.; Lique, F.; Melosso, M.; Puzzarini, C. Collisional excitation of PO^+ by para-H_2: potential energy surface, scattering calculations, and astrophysical applications. *Mon. Not. R. Astron. Soc.* **2023**, *527*, 2279−2287.
(5) Chahal, P.; Kushwaha, A.; Dhilip Kumar, T. Inelastic scattering of PO^+ by H_2 at interstellar temperatures. *Mon. Not. R. Astron. Soc.* **2024**, *534*, 2030−2036.
(6) Roueff, E.; Lique, F. Molecular Excitation in the Interstellar Medium: Recent Advances in Collisional, Radiative, and Chemical Processes. *Chem. Rev.* **2013**, *113*, 8906−8938.
(7) Adler, T. B.; Knizia, G.; Werner, H.-J. A Simple and Efficient CCSD(T)-F12 Approximation. *J. Chem. Phys.* **2007**, *127*, 221106.
(8) Knizia, G.; Adler, T. B.; Werner, H.-J. Simplified CCSD(T)-F12 Methods: Theory and Benchmarks. *J. Chem. Phys.* **2009**, *130*, No. 054104.
(9) Peterson, K. A.; Adler, T. B.; Werner, H.-J. Systematically Convergent Basis Sets for Explicitly Correlated Wavefunctions: The Atoms H, He, B−Ne, and Al−Ar. *J. Chem. Phys.* **2008**, *128*, No. 084102.
(10) Dunning, T. H., Jr; Peterson, K. A.; Wilson, A. K. Gaussian basis sets for use in correlated molecular calculations. *X. The atoms aluminum through argon revisited. The Journal of Chemical Physics* **2001**, *114*, 9244−9253.
(11) Huber, K. *Molecular Spectra and Molecular Structure: IV. Constants of Diatomic Molecules*; Springer Science & Business Media, 2013.
(12) Petrmichl, R. H.; Peterson, K. A.; Woods, R. C. The microwave spectrum of PO^+: Comparison to SiF^+. *J. Chem. Phys.* **1991**, *94*, 3504−3510.
(13) Faure, A.; Jankowski, P.; Stoecklin, T.; Szalewicz, K. On the importance of full-dimensionality in low-energy molecular scattering calculations. *Sci. Rep.* **2016**, *6*, 28449.
(14) Werner, H.; Knowles, P.; Knizia, G.; Manby, F.; Schütz, M. Wiley Interdiscip. *Rev.: Comput. Mol. Sci.* **2012**, *2*, 242−253.
(15) Werner, H.-J.; Knowles, P. J.; Knizia, G.; Manby, F. R.; Schütz, M.; Celani, P.; Györffy, W.; Kats, D.; Korona, T.; Lindh, R.; *Molpro, Version 2015.1, A General-Purpose Quantum Chemistry Program*, 2015, http://www.molpro.net (accessed: 2025-05-28).
(16) Weigend, F. A fully direct RI-HF algorithm: Implementation, optimized auxiliary basis sets, demonstration of accuracy and efficiency. *Phys. Chem. Chem. Phys.* **2002**, *4*, 4285−4291.
(17) Shuai, Q.; de Jongh, T.; Besemer, M.; van der Avoird, A.; Groenenboom, G. C.; van de Meerakker, S. Y. T. Experimental and theoretical investigation of resonances in low-energy NO−H_2 collisions. *J. Chem. Phys.* **2020**, *153*, 244302.
(18) Loreau, J.; Kalugina, Y. N.; Faure, A.; van der Avoird, A.; Lique, F. Potential Energy Surface and Bound States of the H_2O−HF Complex. *J. Chem. Phys.* **2020**, *153*, 214301.
(19) Tonolo, F.; Bizzocchi, L.; Melosso, M.; Lique, F.; Dore, L.; Barone, V.; Puzzarini, C. An Improved Study of HCO^+ and He System: Interaction Potential, Collisional Relaxation, and Pressure Broadening. *J. Chem. Phys.* **2021**, *155*, 234306.
(20) Hays, B. M.; Gupta, D.; Guillaume, T.; Abdelkader Khedaoui, O.; Cooke, I. R.; Thibault, F.; Lique, F.; Sims, I. R. Collisional excitation of HNC by He found to be stronger than for structural isomer HCN in experiments at the low temperatures of interstellar space. *Nat. Chem.* **2022**, *14*, 811−815.
(21) Raghavachari, K.; Trucks, G. W.; Pople, J. A.; Head-Gordon, M. A fifth-order perturbation comparison of electron correlation theories. *Chem. Phys. Lett.* **1989**, *157*, 479−483.
(22) Boys, S. F.; Bernardi, F. The Calculation of Small Molecular Interactions by the Differences of Separate Total Energies. Some Procedures with Reduced Errors. *Mol. Phys.* **1970**, *19*, 553−566.
(23) Meyer, H.-D.; Manthe, U.; Cederbaum, L. S. The Multi-Configurational Time-Dependent Hartree Approach. *Chem. Phys. Lett.* **1990**, *165*, 73−78.
(24) Manthe, U.; Meyer, H.-D.; Cederbaum, L. S. Wave-Packet Dynamics within the Multiconfiguration Hartree Framework: General Aspects and application to NOCl. *J. Chem. Phys.* **1992**, *97*, 3199−3213.
(25) Meyer, H. D.; Gatti, F.; Worth, G. A., Eds.; *Multidimensional Quantum Dynamics: MCTDH Theory and Applications*; Wiley-VCH: Weinheim, 2009.
(26) Beck, M. H.; Jäckle, A.; Worth, G. A.; Meyer, H. D. The multiconfiguration time-dependent Hartree (MCTDH) method: a highly efficient algorithm for propagating wavepackets. *Phys. Rep.* **2000**, *324*, 1−105.
(27) Bacić, Z.; Light, J. C. Highly excited vibrational levels of "floppy" triatomic molecules: A discrete variable representation−Distributed Gaussian approach. *J. Chem. Phys.* **1986**, *85*, 4594.
(28) Bacić, Z.; Light, J. C. Accurate localized and delocalized vibrational states of HCN/HNC. *J. Chem. Phys.* **1987**, *86*, 3065.
(29) Light, J. C.; Carrington, T., Jr. Discrete variable representations and their utilization. *Adv. Chem. Phys.* **2000**, *114*, 263−310.
(30) Ndengué, S. A.; Scribano, Y.; Benoit, D. M.; Gatti, F.; Dawes, R. Intermolecular rovibrational bound states of H_2O-H_2 dimer from a MultiConfiguration Time Dependent Hartree approach. *Chem. Phys. Lett.* **2019**, *715*, 347−353.
(31) Tela, H. T.; Quintas-Sánchez, E.; Dubernet, M.-L.; Scribano, Y.; Dawes, R.; Gatti, F.; Ndengué, S. Rovibrational states calculations of the H_2O-HCN heterodimer with the multiconfiguration time dependent Hartree method. *Phys. Chem. Chem. Phys.* **2023**, *25*, 31813−31824.
(32) Meyer, H.-D.; Gatti, F.; Worth, G. A. *Multidimensional Quantum Dynamics: MCTDH Theory and Applications*; John Wiley & Sons, 2009.
(33) Doriol, L. J.; Gatti, F.; Iung, C.; Meyer, H.-D. Computation of Vibrational Energy Levels and Eigenstates of Fluoroform Using the Multiconfiguration Time-Dependent Hartree Method. *J. Chem. Phys.* **2008**, *129*, 224311.
(34) Ndengué, S. A.; Dawes, R.; Gatti, F.; Meyer, H.-D. Resonances of HCO computed using an approach based on the multi-configuration time-dependent Hartree method. *J. Phys. Chem. A* **2015**, *119*, 12043−12051.
(35) Meyer, H.-D.; Le Quéré, F.; Léonard, C.; Gatti, F. Calculation and selective population of vibrational levels with the Multi-configuration Time-Dependent Hartree (MCTDH) algorithm. *Chem. Phys.* **2006**, *329*, 179−192.
(36) Meyer, H.-D.; Worth, G. A. Quantum molecular dynamics: propagating wavepackets and density operators using the multi-configuration time-dependent Hartree method. *Theor. Chem. Acc.* **2003**, *109*, 251−267.
(37) Meyer, H.-D. Introduction to MCTDH. *Lecture Notes* **2011**.
(38) Gatti, F.; Otto, F.; Sukiasyan, S.; Meyer, H.-D. Rotational excitation cross sections of para-H2+ para-H_2 collisions. A full-dimensional wave-packet propagation study using an exact form of the kinetic energy. *J. Chem. Phys.* **2005**, *123*, 1743311.
(39) Otto, F.; Gatti, F.; Meyer, H.-D. Rotational excitations in para-H2+ para-H_2 collisions: Full-and reduced-dimensional quantum wave packet studies comparing different potential energy surfaces. *J. Chem. Phys.* **2008**, *128*, No. 064305.
(40) Ndengue, S. A.; Dawes, R.; Gatti, F. Rotational Excitations in CO−CO Collisions at Low Temperature: Time-Independent and Multiconfigurational Time-Dependent Hartree Calculations. *J. Phys. Chem. A* **2015**, *119*, 7712−7723.
(41) Gatti, F.; Iung, C.; Menou, M.; Justum, Y.; Nauts, A.; Chapuisat, X. Vector parametrization of the n-atom problem in quantum mechanics. I. Jacobi vectors. *J. Chem. Phys.* **1998**, *108*, 8804−8820.

(42) Gatti, F.; Iung, C.; Menou, M.; Chapuisat, X. Vector parametrization of the N-atom problem in quantum mechanics. II. Coupled-angular-momentum spectral representations for four-atom systems. *J. Chem. Phys.* **1998**, *108*, 8821−8829.

(43) Jennings, D.; Brault, J. The ground state of molecular hydrogen. *J. Mol. Spectrosc.* **1983**, *102*, 265−272.

(44) Faure, A.; Lique, F.; Wiesenfeld, L. Collisional excitation of HC_3N by para-and ortho-H_2. *Mon. Not. R. Astron. Soc.* **2016**, *460*, 2103−2109.

(45) Vindel-Zandbergen, P.; Kedziera, D.; Żółtowski, M.; Kłos, J.; Żuchowski, P.; Felker, P. M.; Lique, F.; Bačić, Z. H_2O−HCN Complex: A New Potential Energy Surface and Intermolecular Rovibrational States from Rigorous Quantum Calculations. *J. Chem. Phys.* **2023**, *159*, 174302.

(46) van der Avoird, A.; Nesbitt, D. Rovibrational states of the H_2O-H_2 complex: An ab initio calculation. *J. Chem. Phys.* **2011**, *134*, No. 044314.

(47) Wang, X.-G.; Carrington, T. Theoretical Study of the Rovibrational Spectrum of H_2O−H_2. *J. Chem. Phys.* **2011**, *134*, No. 044313.

(48) Hutson, J. M.; *BOUND Computer Code, Version 5*, Distributed by Collaborative Computational Project No. 6 of the Science and Engineering Research Council (UK); Science and Engineering Research Council, 1993

(49) Hutson, J. M. Coupled channel methods for solving the bound-state Schrödinger equation. *Comput. Phys. Commun.* **1994**, *84*, 1−18.

(50) Orek, C.; Umiński, M.; Kłos, J.; Lique, F.; Zuchowski, P. S.; Bulut, N. NO^++ H_2: Potential energy surface and bound state calculations. *Chem. Phys. Lett.* **2021**, *771*, No. 138511.

(51) Jankowski, P.; McKellar, A.; Szalewicz, K. Theory untangles the high-resolution infrared spectrum of the ortho-H_2-CO van der Waals complex. *science* **2012**, *336*, 1147−1150.

(52) Denis-Alpizar, O.; Kalugina, Y.; Stoecklin, T.; Vera, M. H.; Lique, F. A new ab initio potential energy surface for the collisional excitation of HCN by para-and ortho-H_2. *J. Chem. Phys.* **2013**, *139*, 224301.

(53) Castro-Juárez, E.; Wang, X.-G.; Carrington, T.; Quintas-Sánchez, E.; Dawes, R. Computational study of the ro-vibrational spectrum of CO−CO_2. *J. Chem. Phys.* **2019**, *151*, No. 084307.

https://doi.org/10.1021/acs.jpca.5c02638
J. Phys. Chem. A 2025, 129, 6247−6260